PHYSICAL REVIEW C VOLUME 5, NUMBER 2 FEBRUARY 1972

Proton Spin-Flip Probability in Inelastic Scattering on ^{120}Sn and ^{124}Sn at 30 MeV*

R. H. Howell† and A. I. Galonsky
Cyclotron Laboratory, Physics Department, Michigan State University, East Lansing, Michigan 48823
(Received 15 September 1971)

Proton spin flip in the excitation of the first 2^+ states in ^{120}Sn and ^{124}Sn has been measured at 30 MeV using the $(p, p'\gamma)$ coincidence technique. The data are fit by the distorted-wave Born-approximation (DWBA) collective model using the full Thomas spin-orbit coupling term and the DWBA microscopic model using a real interaction. The effect of adding an imaginary part to the microscopic interaction was investigated with respect to the present spin-flip data and published asymmetry data. It is concluded that such a term can be important.

I. INTRODUCTION

In order to learn about the spin-dependent part of the interaction in an inelastic scattering reaction there are various measurements possible. The angular distribution of the cross section, asymmetry, polarization, and in special cases the spin flip may all be measured. The probability of a spin-flip event occurring may be measured through the particle-deexcitation γ-ray angular-correlation function with the γ-ray detector fixed perpendicular to the scattering plane.

It can be shown by use of a model-independent theorem[1] that for 0^+ to 1^+ and 0^+ to 2^+ excitations this angular-correlation function is directly proportional to the probability of the projectile changing its spin orientation during the scattering interaction.

Measurements of the angular distributions of the spin-flip probability of scattered protons have been made on the lowest 2^+ states of several even-even targets with mass numbers ranging from 12 to 64 and incident proton energies ranging from 10 to 40 MeV.[2-6] There are also spin-flip data on some of these targets for the scattering of medium-energy helions and deuterons.[7,8]

This report shows angular distributions for the proton spin-flip probility taken on the lowest 2^+ states in ^{120}Sn and ^{124}Sn at 30-MeV bombarding energy. The data are compared with calculations done in the distorted-wave Born-approximation (DWBA) using both the collective model and the microscopic model with a realistic nuclear interaction. The full Thomas form of the distortion of the spin-orbit potential was included in the collective model.[9] The effects of adding an imaginary part to the microscopic interaction were investigated. Asymmetries and cross sections were calculated and compared with data on ^{120}Sn taken at the Rutherford High Energy Laboratory (RHEL) at the same energy.[10]

II. EXPERIMENTAL METHODS

The beam transport and energy-analysis system and the target chamber for this experiment have been previously described.[2] The targets used were isotopically-enriched self-supporting foils of 10 mg/cm^2 for ^{120}Sn (98.4%) and 5 mg/cm^2 for ^{124}Sn (94.7%).

The deexcitation γ rays were detected by a 2-in.-diam by 3-in.-long NaI(Tl) scintillator mounted on a RCA 8575 phototube. The γ-ray energy resolution was 7.5% full width at half maximum (FWHM) for the 662-keV γ ray from a ^{137}Cs source. The face of the detector was 6.125 in. from the target center, giving an average half-angular acceptance of 7.5°. The efficiency–solid-angle produce for this detector was determined in the experimental apparatus by counting the 1.17-MeV γ ray from a calibrated ^{60}Co radioactive source at the normal target position and making a small correction for energy dependence. This product for the full-energy peak was determined to ±6% accuracy to be 1.16×10^{-3} sr for ^{120}Sn ($E_\gamma = 1.17$ MeV) and 1.24×10^{-3} sr for ^{124}Sn ($E_\gamma = 1.13$ MeV). Protons were detected by a single 5-mm-thick Si(Li) detector cooled to dry-ice temperature. A circular collimator 0.7 in. in diameter and 4.6 in. from the center of the target was used to limit the half-angular acceptance to 4°.

Electronics

A block diagram of the electronics system is shown in Fig. 1. Resembling a typical fast-slow coincidence system, this system was designed to minimize pileup and dead-time effects and to allow collection of multiparameter data. To reduce the effects of high γ-ray count rates cable delays or low-dead-time delay amplifiers were used for all timing and logic signals, and short amplifier time constants (100-nsec differentiation and integration)

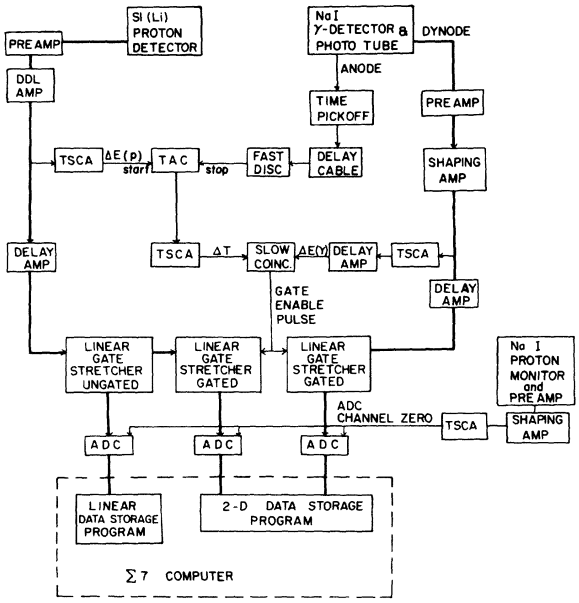

FIG. 1. A block diagram of the electronics. Heavy lines indicate the route of the proton and γ-ray analog signals.

were used for the γ-ray energy pulses.

Fast-timing signals from a timing single-channel analyzer (TSCA) set on the proton amplified pulses started the time-to-amplitude converter (TAC). Delayed signals from an inductive pickup coupled to the anode of the γ-ray detector phototube were used to stop the TAC.

A typical time spectrum is shown in Fig. 2. TAC starts were selected from protons scattered from states of 0- to 3-MeV excitation in the tin target. The spectrum shown has passed through a linear gate enabled by a TSCA which selected pulses between 0.7 and 1.5 MeV in the γ-ray energy spectrum. The large peaks are due to the pulsed nature of the cyclotron beam which has a period of 61.5 nsec at 30 MeV. Structure within these peaks corresponds to starts from protons scattering from separate energy levels in the tin nucleus. This structure is due to charge-collection effects integrated into the double-delay-line-amplified (DDL AMP) proton pulse. The peak containing true coincidence events is identified by an increase in the starts from excited states, while elastic events contribute evenly to all peaks. The FWHM of the total peak is 22 nsec.

Events from the true coincidence peak were selected by a TSCA. A slow coincidence was required between the output of the TSCA set on the fast-time spectrum and the output of the TSCA set on the γ-ray energy spectrum. The output of the slow-coincidence unit was used to enable the linear gate stretchers (LGS). Pairs of coincident pulses were passed by the LGS for pulse-height analysis. These pulses were converted by two analog-to-digital converters (ADC) and stored "on-line" in a 128×128-channel array in the core of the XDS Sigma-7 computer. The coincident particle–γ-ray event was displayed on an oscilloscope and markers were set to extract one-dimensional spectra.

Ungated, stretched proton pulses were analyzed by a third ADC and after conversion were stored in a 1024-channel spectrum in the core of the XDS Sigma-7 computer. Collection of this singles spectrum for the whole run at each angle provided a convenient normalization for the coincidence data. The selected one-dimensional coincidence spectra, the two-parameter coincidence array, and the singles proton spectrum were stored on cards for

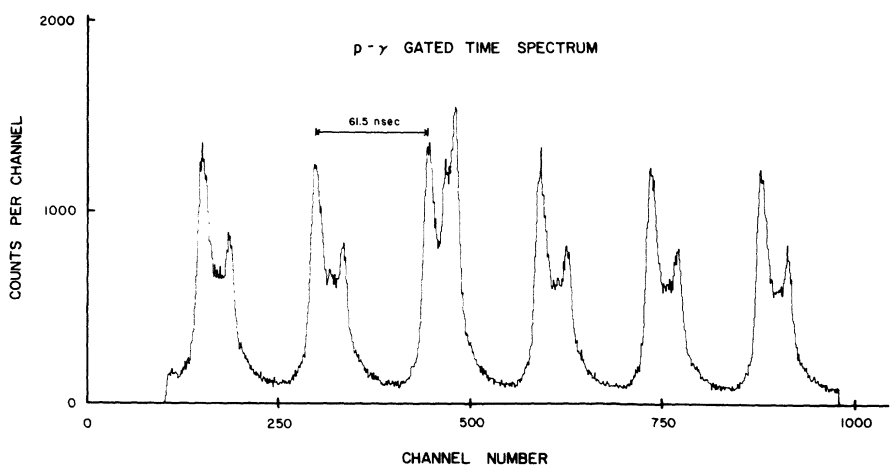

FIG. 2. Proton–γ-ray time spectrum. Start pulses come from the proton TSCA, the stop pulses from the γ-ray fast discriminator. The TSCA's were set so that $0.7 \le E_\gamma \le 1.5$ MeV. The true peak is identified by the increased height on the right side of the peak.

later analysis. Proton starts, gated γ-ray stops, true-coincidence gate enables, and all elastic events in the monitor were separately counted on scalers in order to monitor the course of the experiment and to calculate dead-time corrections.

Data Reduction

The probability for a proton scattered at θ to have its spin flipped is, for infinitesimal detectors,

$$S(\theta)=\frac{8\pi}{5}\,\frac{1}{\epsilon d\Omega}\,\frac{R}{N},$$

where θ is the proton scattering angle, $\epsilon d\Omega$ is the solid-angle–efficiency product, N is the total number of inelastic scattering events to the 2^+ state, and R is the number of real coincidences.

R may be calculated from the formula $R=T_{2^+}-KT_e$, where T_{2^+} (T_e) is the total number of coincidence events from the 2^+ (ground) state. The scaling factor K is the ratio of singles 2^+ events to singles elastic events taken in the same proton energy bins as used in the analysis of the coincidence data.

Total coincidences were determined by summing the coincident counts in the two-parameter array which corresponds to the γ-ray photopeak and the 2^+ proton peak. The number of accidential counts, KT_e, was determined by summing counts in the same γ-ray energy range which corresponds to the proton elastic peak, and scaling the counts by the singles ratio K.

The statistical standard error, $\delta S(\theta)$, associated with $S(\theta)$ is

$$\delta S(\theta)=\frac{8\pi}{5}\,\frac{1}{\epsilon d\Omega}\,\frac{[T_{2^+}+K^2T_e+T_e^2(\delta K)^2]^{1/2}}{N},$$

where the error in N is small and is neglected.

Writing a formula for $S(\theta)$ in terms of R/N when detectors subtend finite solid angles is not so simple. The radiation pattern for γ rays resulting from a spin-flip ($\Delta m=\pm1$) transition is peaked along the line perpendicular to the scattering plane. Also, the radiation patterns for the non-spin-flip ($\Delta m=0,\pm2$) transitions are zero only along the perpendicular. Thus, to calculate $S(\theta)$ for a finite γ-ray detector one must take the weighted average of the spin-flip γ-ray radiation pattern over the detector solid angle and subtract the contribution of real coincidences from non-spin-flip transitions. The number of real coincidences from non-spin-flip transitions is a function of the relative populations of the $m=0,\pm2$ sublevels of the excited 2^+ state. The position of the particle-detector aperture defines the scattering plane. An aperture of finite size, however, will define an envelope of scattering planes. Each scattering plane in the envelope is weighted by the fraction of the total

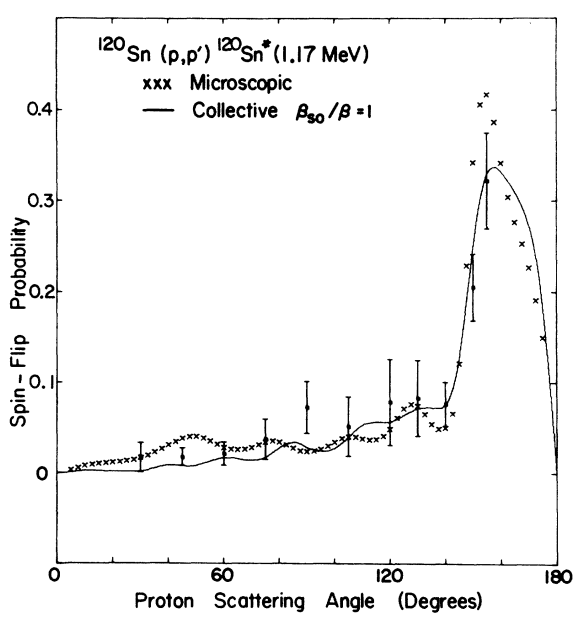

FIG. 3. Spin-flip probability for ^{120}Sn. The data have been corrected for the use of finite detector apertures. The curves are the collective model with a full Thomas term (solid line) and the microscopic model with the KK force (x's).

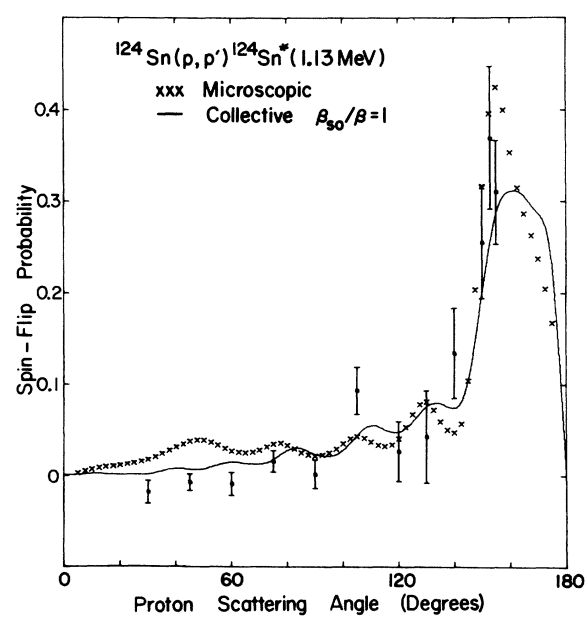

FIG. 4. Spin-flip probability for ^{124}Sn. The correction for finite detector apertures reduces the value of the data at forward angles. The curves are the collective model with a full Thomas term (solid line) and the microscopic model with the KK force (x's).

TABLE I. Becchetti and Greenlees optical-model parameters (Ref. 14).

	V	W_V	W_D	V_{so}	r_R	a_R	r_I	a_I	r_{so}	a_{so}	r_C
^{120}Sn	52.46	3.9	6.20	6.2	1.17	0.75	1.32	0.627	1.01	0.75	1.20
^{124}Sn	53.05	3.9	6.62	6.2	1.17	0.75	1.32	0.645	1.01	0.75	1.20

accepted particle flux contributed from that plane. The size of the envelope depends on the scattering angle, becoming larger as the detector angle changes from 90° and encompassing all scattering planes at 0 and 180°.

In this experiment $S(\theta)$ was calculated with a formula[8] which is a function of scattering angle, the ratio of the $m=+2$ to the $m=0$ substate population, the half-angle acceptance of the proton and γ-ray detectors, the geometry of the proton-detector aperture, and the dependence of the γ-ray-detector efficiency on the angle of incidence of the γ ray. The derivation of this formula assumes that the $m=+2$ and $m=-2$ sublevels are populated equally. Figures 3 and 4 show the spin-slip-probability data for ^{120}Sn and ^{124}Sn. The data were calculated with a ratio of $m=2$ to $m=0$ substate populations (q) of 1.0. The errors shown are the statistical error and an estimate of the error generated in choosing $q=1.0$ added in quadrature. Since the actual substate populations are unknown, the values of $S(\theta)$ calculated at each angle with $q=0$ and $q=\infty$ represent the limits of possible values of $S(\theta)$. Two-thirds the difference between these limiting values was used as an estimate of the total uncertainty generated in the arbitrary choice of q. This contribution doubled the error on some forward-angle data where the statistical error is small, but increased the error on the backward-angle data by only about 10% of the statistical error.

Calculating $S(\theta)$ with this formula resulted in lower values than those obtained by assuming that the detectors had infinitesimal apertures. This is especially true for the forward-angle ^{124}Sn data where the choice of any value of q greater than zero results in negative values for $S(\theta)$. The data on ^{120}Sn and ^{124}Sn are quite similar. The main differences between the two isotopes is seen at angles forward of 75° where the ^{120}Sn data are consistantly higher than that for ^{124}Sn.

III. ANALYSIS

Theoretical analysis of the data was carried out in the DWBA. Both collective and microscopic interaction models were used.

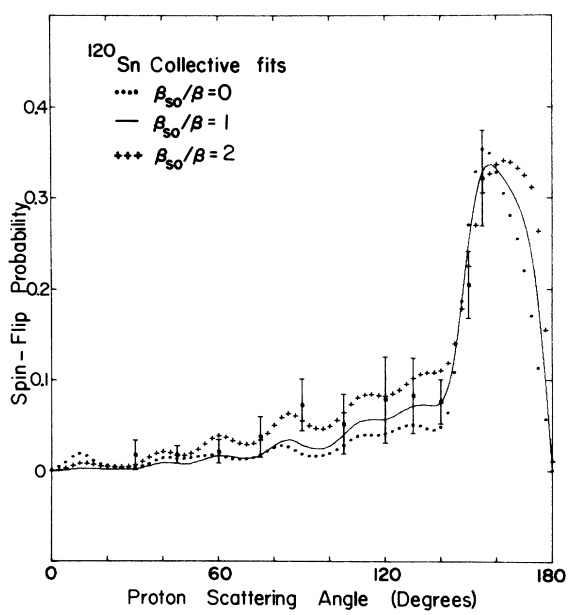

FIG. 5. Collective-model calculations with the full Thomas term. Increasing the strength of the spin-orbit deformation from 0 to 2β does not greatly change the quality of the fit.

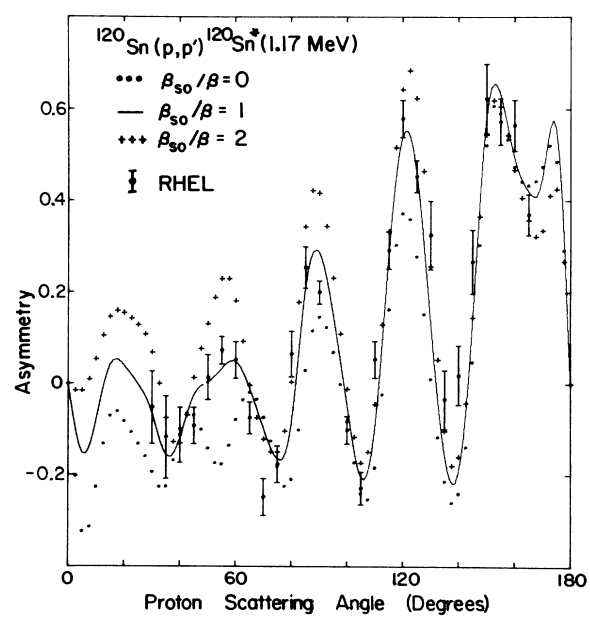

FIG. 6. Collective-model calculations of the asymmetry with the full Thomas term. Increasing the strength of the spin-orbit deformation from 0 to 2β has the greatest effect at forward angles where the central collective model is in least agreement with the data (Ref. 10).

Optical Model

The distorted waves were obtained through the usual optical-model potential:

$$U(r)=U_C-Vf(r,r_R,a_R)-i\left(W_V-4aW_D\frac{d}{dr}\right)f(r,r_I,a_I)+\left(\frac{\hbar}{m_\pi c}\right)^2V_{so}\frac{1}{r}\frac{d}{dr}f(r,r_{so},a_{so}).$$

The Coulomb potential, U_C, was taken to be that of a uniformly charged sphere with radius $r_C A^{1/3}$. The functions $f(r,r_x,a_x)$ are the Woods-Saxon radial distributions.

Several sets of optical-model parameters exist for ^{120}Sn at 30 MeV.[11-14] The parameters used in the following calculations are the best-fit parameters of Becchetti and Greenlees[14] which were obtained by a simultaneous fit of cross-section and polarization data of many nuclei at several energies.

These parameters have the advantage of being easily extended to ^{124}Sn with isotopic dependence systematically included. The values used are shown in Table I. These values do not differ greatly from best-fit parameters obtained by analysis of ^{120}Sn data alone.

Collective Model

Collective-model calculations were done including a deformed spin-orbit potential with the full Thomas form developed by Sherif and Blair.[9] The deformation of the Thomas form of the spin-orbit potential can be written as

$$\Delta U_{so}=\Delta U(1)+\Delta U(2),$$

where for an excited state with spin I,

$$\Delta U(1)=\frac{\beta_I^{so}R_{so}^0}{\sqrt{2L+1}}\left(\frac{\hbar}{m_\pi c}\right)^2V_{so}\frac{1}{r}\frac{\partial^2}{\partial r\partial R_{so}}fY_I^{*M}(\theta,\phi)\vec{\sigma}\cdot\vec{L},$$

$$\Delta U(2)=\frac{\beta_I^{so}R_{so}^0}{\sqrt{2L+1}}\left(\frac{\hbar}{m_\pi c}\right)^2\times V_{so}\frac{\partial}{\partial R_{so}}f\vec{\sigma}\cdot\left[\nabla Y_I^{*M}(\theta,\phi)\times\frac{1}{i}\nabla\right],$$

where

$$f=[1+\exp-(r-R_{so})/a_{so})]^{-1}$$

and R_{so}^0 is the undeformed nuclear radius.

The sum of the terms $\Delta U(1)$ and $\Delta U(2)$ includes all ths spin-orbit strength generated through the usual first-order treatment of the deformation of the optical potential in the collective model. This sum is the full Thomas term.

All collective-model calculations were done with a computer code written by Sherif which includes the full Thomas form with a separate deformation strength as a free parameter. Coulomb excitation was included in all calculations. The strength of the spin-orbit deformation (β_{so}) relative to the main-potential deformation (β) was varied and the calculations were compared with the measured spin-flip, asymmetry, and cross-section angular distributions for ^{120}Sn and with the spin-flip angular distribution for ^{124}Sn. Collective-model fits to the spin-flip and asymmetry data are shown in Figs. 5 and 6 for values β_{so}/β of 0, 1, 2.

The spin-flip and cross-section calculations are not as sensitive to the relative strength of the deformation as the asymmetry calculations. The fits to the asymmetry data are most sensitive at the forward angles where the phase of the calculated asymmetry is changed by including the deformed spin-orbit strength. Backward angles exhibit only changes in amplitude. Of the fits shown for the asymmetry, the best is for $\beta_{so}=\beta$. The spin-flip fits on either target are too insensitive to β_{so} for a choice to be made. Varying β_{so} relative to β from 0 to 2 leaves the values of the total (p,p') cross section essentially unchanged. The value of β obtained by normalizing the theoretical integrated cross section to the experimental integrated cross section is 0.133. The value is about 10% higher than the value extracted from experimental $B(E2)$ values.[15]

Microscopic Model

Microscopic calculations were done using the long-range part of the Kallio-Koltveit (KK) potential[16] for the projectile-target interaction. This is a central force. The targets were described by the quasiparticle wave functions of Clement and Baranger[17] which include 27 neutron and six proton configurations. Exchange effects were included using the zero-range approximation suggested by Petrovich *et al.*[16] The microscopic fits to the asymmetry and cross section are shown in Figs. 7 and 8. The microscopic spin-flip calculations may be seen in Figs. 3 and 4.

The spin-flip calculations for ^{120}Sn and ^{124}Sn are in reasonable agreement with the data. No strong isotopic differences are evident in the calculations for either case. The ^{120}Sn cross section is too low at the first maximum, but the shape is in general agreement with the data. The ^{120}Sn asymmetry fit is much worse than in the collective case. The values are too low throughout the whole angular range of the fit. Only the phase of the oscillations continues to agree with the data.

The form factor in the microscopic calculations is real. In order to see if some of the discrepancy in the microscopic fit to the asymmetry is due to omitting the imaginary part of the form factor or

to the lack of an $\vec{l}\cdot\vec{s}$ term in the force two calculations were performed.

The first calculation used only the real part of the collective-model form factor with $\beta_{so}/\beta = 0$. The second calculation used the real KK form factor plus the imaginary part of the collective form factor. The addition of an imaginary part to the microscopic KK form factor greatly improves the fit to the asymmetry data, while the real collective-model form factor gives poor agreement and is quite similar to the real microscopic calculation as seen in Fig. 7. This indicates that part of the failure of the microscopic calculation to fit the asymmetry data at most angles in this case lies in the use of a real interaction.

While not as pronounced, the addition of an imaginary term to the real microscipic form factor also gives some improvement to the fit to the inelastic cross section. The value of the calculated cross section is raised at the first maximum to the value of the experimental data. Although the data do not indicate as much structure in the angular distribution as does the calculation, the over-all fit to the cross section is somewhat improved, as seen in Fig. 8.

The spin-flip calculations with the real microscopic form factor are not changed significantly in shape or magnitude by the addition of an imaginary part to the form factor. Differences between the microscopic and collective-model calculations here seem to be dependent on the details of the real form factor.

IV. SUMMARY

Spin-flip probabilities for the excitation of the first 2^+ states in ^{120}Sn and ^{124}Sn have been measured for inelastic proton scattering at 30 MeV. The spin-flip data for both isotopes are quite similar. Both show the peak at the backward angles which is characteristic in medium-energy spin-flip data taken on lighter nuclei.[2-8] The tin spin-flip, cross-section,[10] and asymmetry data have been analyzed with both macroscopic and microscopic DWBA models.

For the collective model, fits to the cross section are reasonably good. However, the calculated curve shows somewhat more structure than is evident in the data. Use of a deformed spin-orbit term is important, but no more so than the imaginary part of the collective form factor for the asymmetry data. It has little effect on either the spin-flip or cross-section calculations. The fit to the ^{120}Sn spin-flip data is quite good over the whole angular range. The fit to ^{124}Sn spin-flip is good for the backward-angle peak but the low forward-angle values are not predicted. Little structure at forward angles is predicted or seen in the spin-flip data for either target.

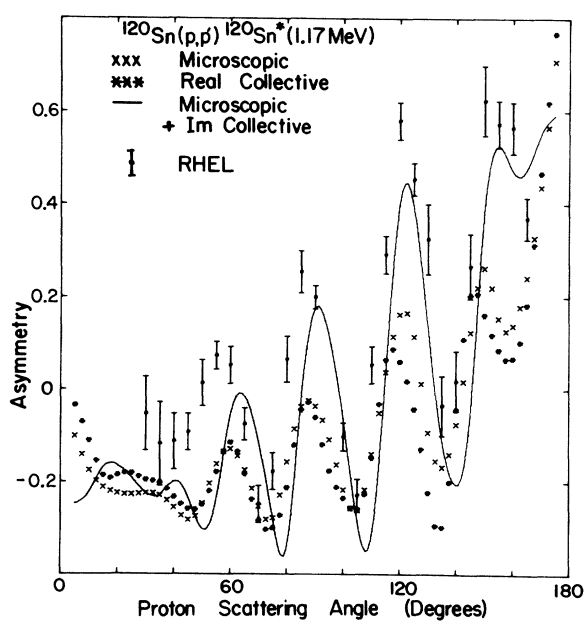

FIG. 7. The fits to the asymmetry with the real microscopic force (x's) and real part of the collective model (*'s) are degraded at all angles. Adding an imaginary part to the microscopic form factor (solid line) improves the fit over most of the angular range.

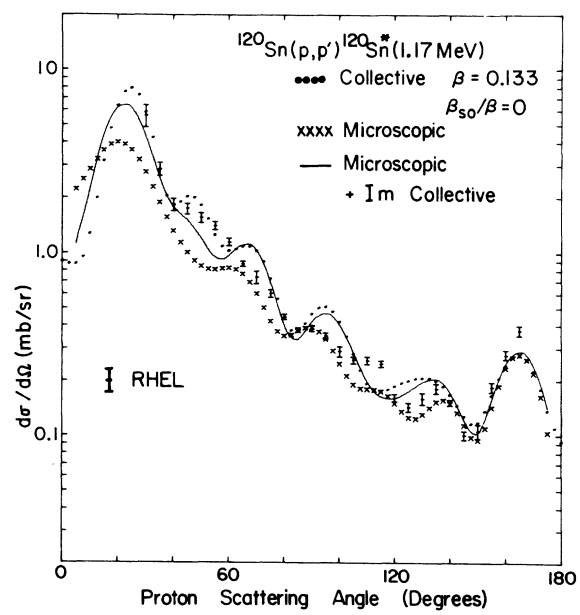

FIG. 8. Adding an imaginary part to the real microscopic form factor (solid line) improves the fit to the cross section over that of the real microscopic form factor alone (x's). The complex collective model (dots) without spin-orbit deformation also fits the data (Ref. 10) well.

The shape and magnitude of the cross-section and spin-flip predictions are reasonable using the Clement and Baranger quasiparticle wave functions. The predicted spin flip has a higher value at the backward peak than for the collective-model case. However, it still shows agreement with the data. No isotopic changes were evident in comparing spin-flip predictions for ^{120}Sn and ^{124}Sn.

The asymmetry was not fitted very well using a real KK interaction. The addition of an imaginary term to the form factor greatly improves the asymmetry prediction and shows some improvement in the fit to the cross section. An $\vec{l}\cdot\vec{s}$ term in the microscopic interaction would probably improve the results further. The spin-flip prediction is unchanged in making the form factor complex.

---

*Work supported by the National Science Foundation.

†Present address: Lawrence Radiation Laboratory, Livermore, California 94550.

[1]A. Bohr, Nucl. Phys. 10, 486 (1959).

[2]J. J. Kolata and A. Galonsky, Phys. Rev. 182, 1073 (1969).

[3]F. H. Schmidt, R. E. Brown, J. B. Gerhart, and W. A. Kolasinski, Nucl. Phys. 52, 353 (1964).

[4]W. A. Kolasinski, J. Eenmaa, F. H. Schmidt, H. Sherif, and J. R. Tesmer, Phys. Rev. 180, 1006 (1969).

[5]R. O. Ginaven, E. E. Gross, J. J. Malanify, and A. Zucker, Phys. Rev. Letters 21, 552 (1968).

[6]D. L. Hendrie, C. Glashausser, J. M. Moss, and J. Thirion, Phys. Rev. 186, 1188 (1969).

[7]D. M. Patterson and J. G. Cramer, Phys. Letters 27B, 373 (1968).

[8]H. H. Hippelein, R. Jahr, J. A. H. Pfleger, F. Rott, and H. M. Vieth, Nucl. Phys. A142, 369 (1970).

[9]H. Sherif and J. S. Blair, Phys. Letters 26B, 489 (1968); H. Sherif, Ph.D. thesis, University of Washington, 1968 (unpublished).

[10]O. Karban, P. D. Greaves, V. Hnizdo, J. Lowe, and G. W. Greenlees, Nucl. Phys. A147, 461 (1970).

[11]G. W. Greenlees and G. J. Pyle, Phys. Rev. 149, 836 (1966).

[12]G. R. Satchler, Nucl. Phys. A92, 273 (1967).

[13]G. W. Greenlees, Phys. Rev. C 2, 1063 (1970).

[14]E. D. Becchetti and G. W. Greenlees, Phys. Rev. 182, 1190 (1969).

[15]T. H. Curtis, R. A. Eisenstein, D. W. Madsen, and C. K. Bockelman, Phys. Rev. 184, 1162 (1969).

[16]F. Petrovich, H. McManus, V. A. Madsen, J. Atkinson, Phys. Rev. Letters 22, 895 (1969); F. Petrovich, Ph.D. thesis, Michigan State University, 1970 (unpublished); private communication.

[17]D. M. Clement and E. U. Baranger, Nucl. Phys. A120, (1968); and private communication.